Rheologica Acta manuscript No.
(will be inserted by the editor)

New Insights on Fumed Colloidal Rheology - Shear Thickening and Vorticity Aligned Structures in Flocculating Dispersions

Ajay Singh Negi · Chinedum O. Osuji

Received: date / Accepted: date

Abstract We investigate the rheology of dilute dispersions of fumed colloidal particles with attractive interactions in hydrocarbon liquids. Surprisingly, these systems display shear thickening due to the breakdown of densified flocs and a concomitant increase in the effective volume fraction of the fractal particles in the fluid. We show that this shear thickening is controlled by a critical stress and accompanied by a positive increase in the first normal stress difference, N_1 at the shear thickening transition. This is in contrast to the well-known hydrocluster mechanism of shear thickening in concentrated hard-sphere and repulsive systems. Gel elasticity depends strongly on the stress applied to suspensions in pre-shear, scaling roughly as $G' \sim \sigma^2_{pre-shear}$. We propose a simple model to account for these results in terms of the cluster number density determined by the pre-shear stress. At low shear rates, vorticity aligned aggregates are present at $\dot{\gamma} \approx 10^0$ s^{-1}. In this regime the system displays a small but noticeable increase in viscosity on increasing shear rate. We investigate the effect of tool roughness and find that wall slip is not responsible for the observed phenomena. Instead, the increase in the apparent viscosity results from increased flow resistance due to the presence of gap-spanning log-like flocs in rolling flow.

A. Negi
Department of Chemical Engineering, Yale University, New Haven, CT 06511
Tel.: 203-436-4059
E-mail: ajay.negi@yale.edu

C. Osuji
Department of Chemical Engineering, Yale University, New Haven, CT 06511
Tel.: 203-432-4357
Fax: 203-432-4387
E-mail: chinedum.osuji@yale.edu

Keywords carbon black · colloidal gels · shear thickening · stress relaxation · flocculation · shear induced structures

PACS 82.70.Dd · 82.70.Gg · 83.60.Rs

1 Introduction

The rheology of colloidal dispersions may be highlighted by the display of shear thickening behavior in which the viscosity of the system grows with increasing shear rate [1]. Such flows are of immense practical concern as they are relevant in the fluid handling of particulate suspensions in a wide variety of processes, ranging from cement mixing to the manufacture of cosmetics and filled polymers [2,3]. Experimental [4–6] and simulation studies [7–9] have considerably advanced the understanding of this phenomenon and shear thickening is now well understood, generally, to arise due to the formation of shear-induced hydroclusters. Briefly, particles are forced towards contact along the compressive axis of the shear flow resulting in enhanced viscous dissipation by fluid flow between particle surfaces with small separations. The critical condition for the onset of shear thickening may be rationalized in terms of a balance between the shear stress forcing particles towards contact and any stabilizing forces which oppose close approach, as in Equation 1 for Brownian spheres

$$\frac{3\pi\eta_o\dot{\gamma}_c a^3}{2h} = -k_B T\frac{\partial \ln g(r)}{\partial r} + F_{rep} \quad (1)$$

where a is the particle radius, $h = r - 2a$ the distance between two particles, $g(r)$ the particle distribution function and η_o the viscosity of the suspending fluid, replaceable by the suspension viscosity, η,

as a way of accommodating many body effects. F_{rep} is the non-Brownian repulsive force between particles that may arise from electrostatic contributions, or the presence of stabilizing polymer brushes on the particle.

In hard sphere and repulsively interacting colloidal suspensions, hydrocluster formation leading to shear thickening is commonly observed at high loadings, $\varphi \gtrsim 40\%$. The increase of viscosity with shear rate may be smooth and continuous, or discontinuous in which case a dramatic jamming of the system can occur with the viscosity diverging as the particles are forced into contact in clusters with system-size dimensions. By contrast, shear thickening of this nature is not known nor predicted for flocculating colloidal systems, i.e. systems with substantial attractive interactions [1,10,11]. In such gel forming materials, flow curves exhibit monotonic shear thinning behavior. Viewed from the perspective provided by Equation 1, this is surprising as the critical stress for hydrocluster formation should be expected to decrease with increasing strength of attraction between particles or decreasing F_{rep}, that is, as the barrier to hydrocluster formation decreases. A systematic study of the effect of interaction strength was conducted in depletion induced gels where fine control over the interaction strength is provided by the polymer depletant concentration [10]. Here, the critical shear stress at the onset of shear thickening is seen in fact to decrease as a function of interaction strength, but crucially, the extent of shear thickening also decreases until it completely vanishes for systems with substantial interactions, sufficiently strong to induce flocculation. An important emerging concept is that hydrocluster formation does in fact occur in aggregating systems, but the resulting increase in the hydrodynamic contribution to the viscosity does not offset the large decrease in the thermodynamic contribution, and so the overall observable is a decrease in viscosity on increasing shear rate, i.e. monotonic shear thinning [10].

Fumed colloidal particles are commodity materials that find application in a great variety of fields. For example, carbon black is used as a pigment in inks and paints and a filler in rubber tires. Fumed silica is widely used as a filler and rheology modifier in gels and rubbers. Fumed alumina finds application in coatings, adhesives and personal care products. Many of these applications fall under the rubric of "pastes," the rheophysics of which have been well reviewed [12]. All are produced via flame processing of an appropriate feedstock (heavy oil, $SiCl_4$, Al_2Cl_6) under specific conditions that results in the production of nano-scale primary particles, ca. 1-10 nm, that collide and sinter in the flame to form larger aggregates. It is these aggregates which are considered the colloidal "particles", with particle sizes ranging generally from $\mathcal{O}(10^{-1})$ to $\mathcal{O}(10^{+1})\mu$m. They are characterized by a fractal dimension, d_f^p, which describes the size dependence of the particle mass as $M \sim R^{d_f^p}$. The smaller the fractal dimension, the more open or porous is the particle structure. Typical dimensions are anywhere from 2 to 2.8 as characterized by x-ray scattering [13,14]. Unsurprisingly, the suspension rheology of these structured particles is of considerable importance in the handling and processing of the particles themselves and of the many complex fluids that incorporate them in their formulation.

Considerable attention has been devoted to this topic, as well as to the rheological modification, primarily mechanical reinforcement, of fumed particle filled polymers. Slurries of these particles in purely viscous or inelastic media display qualitatively similar rheology as do their "three-dimensionally full" or "fully solid" counterparts. Under attractive conditions, they aggregate and form gels composed of networks of particle flocs, with an elastic modulus that scales with composition as $G' \sim \varphi^{\alpha}$ [15,16]. The scaling exponent α is a function of the interaction strength between particles, with typical values of $3 \leq \alpha \leq 5$. Under excluded volume or repulsive interactions, no flocculation occurs. The steady flow response shows a Newtonian plateau followed by shear thinning above a critical shear rate. At sufficiently high volume fractions, they exhibit shear thickening due to the formation of hydroclusters as discussed above for solid particles. Notably, the effective volume fraction of the fumed colloidal particles as deduced from the zero-shear viscosity via the Batchelor expression is several factors larger than the nominal volume fraction, calculated on a mass density basis. This is attributed to the large hydrodynamic radius of the fractal aggregates and the entrapment of fluid in the porous particles. Thus, shear thickening attributed to hydrocluster formation has been observed at nominal volume fractions as low as a few percent [11,17]. In parallel to the observation of hydrocluster driven shear thickening in hard-sphere and repulsive fumed particulate systems, shear thickening is not expected under flocculating conditions [11].

Here, we report on the observation of modest shear thickening in flocculating fumed colloidal dispersions of carbon black and alumina in hydrocarbon media. Shear thickening in these systems is driven not by hydrocluster formation but by breakup of dense fractal clusters resulting in an increase in the effective volume fraction of the system, as detailed in our previous publication regarding carbon black in tetradecane solvent [18]. We consider the effect of varying solvent viscosity and present results illustrating that the breakup of clusters

is controlled by a critical stress, and not a critical shear rate. We find a strong correlation between the elastic modulus of gels and the pre-shear stress to which they are subjected, underpinned by the difference in suspension microstructure in the shear thinning vs. shear thickening regimes. These systems display measurable residual stresses on cessation of flow, and we characterize their dynamics as dependent on the pre-shear to which the system is subjected. The microstructure of the shear thickened gels displays a dramatic instability, resulting in the formation of highly anisotropic vorticity aligned aggregates on shear flow, studied here in alumina dispersions. These results shed new light overall on the rheology of fumed colloidal materials and help explain some curious phenomena observed in these materials in past reports [19, 20].

2 Experimental

Carbon black was obtained from Cabot Corporation. The particular grade used, Vulcan X72R, exists as $\approx 0.5\mu m$ diameter particles with a particle fractal dimension $d_f^p = 2.2$ and bulk density $\rho_{carbon} = 1.8$ g/cm^3. Fumed alumina (SpectrAl 100) was also obtained from Cabot with bulk density $\rho_{alumina} = 3.7$ g/cm^3. Tetradecane (Aldrich Chemical Co., $\eta = 2.8$ cPs, $\rho = 0.76$ g/cm^3) and a medium-bodied mineral oil (Aldrich Chemical Co., $\eta = 45$ cPs, $\rho = 0.85$ g/cm^3) were blended in various proportions to provide suspending media of tunable viscosity, according to a logarithmic mixing rule. Under these conditions, i.e. in non-polar solvents, there is no charge on the surface of the particles and so they interact solely via an attractive Van der Waals potential. A concentrated stock of the fumed colloidal particles in the relevant fluid was produced by vortex mixing for about 2 minutes, sonication for another 10-30 minutes and vortexing again for 2 minutes. Samples for measurement were then prepared from the well-mixed stock by dilution, followed by vortexing and sonication.

Rheological characterizations were performed using a combination of unaltered and roughened tool surfaces in cone-plate, parallel plate and Couette geometries. Steady flow characterizations were performed on an ARES LS-1 (Rheometrics) strain controlled instrument, as well as with an MCR301 (Anton-Paar USA) stress-controlled rheometer run in strain control mode. Dynamic data were recorded on the MCR301. The fast hardware-based feedback of this instrument was used to monitor residual stresses on shear rate quenches by observing the applied stress required to keep the sample under constant zero strain. For these experiments, the rheometer was installed on an air-floated table to eliminate vibration of the sample by mechanical room noise. Optical characterization was conducted in strain control in parallel-plate and cone-plate geometries using the MCR301 instrument. A fiber-guided ring light source was positioned together with a CCD camera below the glass plate of the rheometer to permit imaging via reflection off the top tool of the instrument.

All measurements were conducted at 25 °C, with temperature control provided by Peltier elements. For steady flow measurements, two different methods were applied. The first approach involved pre-shearing samples at the highest shear rate to which they would subsequently be exposed, $\approx 1000\text{s}^{-1}$, followed by repeated descending and ascending shear rate sweeps. Alternatively, repeated shear sweeps were performed, but the first ascending sweep data was discarded due to the inconsistent mechanical history involved in handling and loading the sample into the rheometer. Both methods were found to produce consistent, reproducible flow curves in good agreement, and data for steady flow is presented here without additional specification of the pre-shear routine. Equilibration at each data point was ensured by using ≈ 60 s stabilization time, and $\approx$ 10-15 s integration time, with a minimum data density of 10 pts./decade. In the case of measurements conducted on the ARES the data collection time was doubled as two directions of rotation were used at each data point in order to avoid artifacts due to instrument offsets of residual stresses in the samples. It is important to note that the mixing performed on samples, although thorough, served only to macroscopically homogenize the materials. The settling and heterogeneity introduced by the handling and loading of the sample necessitates an appropriate pre-shear after the sample is loaded to ensure consistent results. All samples were checked to verify that edge-fracture, possible in the shear flow of sticky systems, did not occur.

For dynamic measurements, samples were pre-sheared at a fixed rate of 50 s^{-1} for 30 minutes and then pre-sheared at the particular shear rate of interest again for 30 minutes before finally being allowed to sit quiescently for 15 minutes. Following this gelation time, the storage and loss moduli were characterized using a frequency of ω =1 rad/s and strain $\gamma = 0.1\%$, which was within the linear regime as confirmed by dynamic strain sweeps, conducted at $\omega = 1$ rad/s. Frequency sweeps were conducted in the linear regime using the same strain, $\gamma = 0.1\%$.

3 Results and Discussion

3.1 Steady Flow Behavior

The flow curves for carbon black and alumina exhibit qualitatively similar features. The samples exhibit two regimes of increasing viscosity with increasing shear rate, with shear thinning behavior at all other points. The first regime, at lower shear rates, $\sim 10^0$ s^{-1}, features a somewhat irregular, slight increase in viscosity, or at times what appears to be more of a plateau in the flow curve. This will be referred to as the structuring regime. At higher shear rates, in the second regime, the samples shear thicken modestly, with a 2-5X increase in viscosity, as shown for data taken using the cone-plate geometry in Figure 1. This will be referred to as the shear thickening regime. Within the shear thinning regions, both materials exhibit the thixotropy that is commonly encountered in flocculated gels - stepped increases of shear rate result in time-dependent decreases in the viscosity as the material is broken down in the flow [21]. In the shear thickening regime, suspensions display a negative thixotropy as the viscosity increases with time in response to a stepped increase of shear rate.

Correspondingly, samples display thixotropic loops with the viscosity on descending rate sweeps above that at the corresponding shear rate on the ascending arm of the flow curve, Figure 2. The departure of the descending sweep from the ascending curve is, notably, at the peak of the shear thickening regime on the ascending curve.

From our data, we extract the critical shear rates on ascending and descending sweeps, $\dot{\gamma}_c^a$, $\dot{\gamma}_c^d$ and corresponding critical shear stresses, σ_c^a, σ_c^d that denote the transitions to and from shear thickening flow. We find qualitatively different composition scaling of the critical stress and rate on the ascending and descending curves, Figure 3. In particular, $\dot{\gamma}_c^a \sim \varphi^{-1}$, whereas $\dot{\gamma}_c^d \sim \varphi^0$. Correspondingly, $\sigma_c^a \sim \varphi^1$ and $\sigma_c^d \sim \varphi^2$. For the peak viscosity, $\dot{\gamma}_p^a \sim \varphi^{-1}$, whereas $\dot{\gamma}_p^d \sim \varphi^0$. Additionally, $\sigma_p^a \sim \varphi^{1.5}$ and $\sigma_p^d \sim \varphi^{2.5}$. With only 1/3 of a decade in composition range, the actual value of the exponents cannot be robustly determined. However, it is noteworthy that the sum of the absolute values of the exponents is roughly constant for the ascending and descending critical transitions and peaks. This suggests a consistent variation of the critical viscosity and peak viscosities with composition both on the ascending and descending sweeps.

In order to determine whether the transition to shear thickening flow is rate or stress controlled, we examined the flow curves across a number of fluid viscosities. The

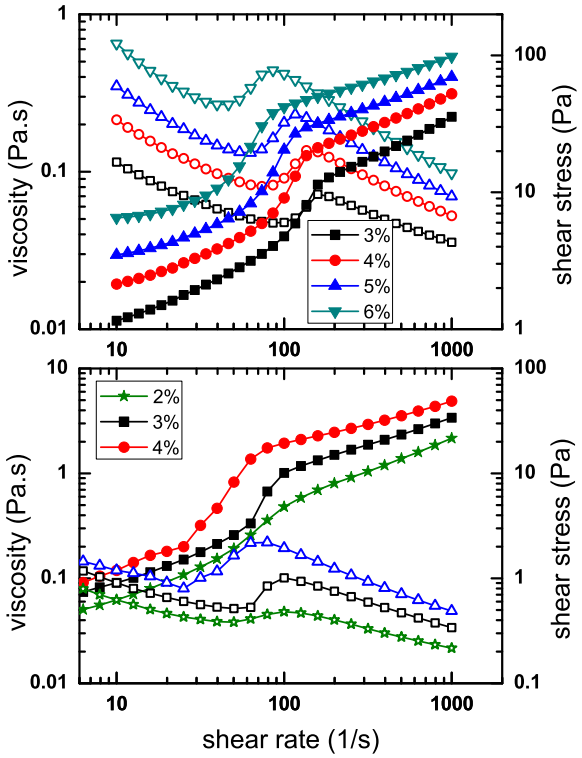

Fig. 1 Steady-state flow curves on ascending rate sweeps on carbon black (top) and alumina (bottom) suspensions in a 3:1 (by weight) mixture of mineral oil with tetradecane. Data were measured on ARES-LS1 instrument using a 2°, 50 mm cone. For the Alumina samples, the tool surfaces were covered with a gritted paper and confirmed the absence of roughness effects in this regime. Filled symbols are stress, open symbols are viscosity.

critical shear rate varied inversely with the viscosity of the solvent, and the data can be rescaled onto a single curve using the hydrodynamic stress, $\sigma_h = \dot{\gamma}\eta_{solvent}$, indicating that shear thickening in these systems is controlled by a critical stress, as seen from the data of Figure 4.

Along with the viscosity characterization, steady flow experiments provided measurements of the normal stress behavior. It should be noted that normal stress differences in colloidal suspensions are notoriously difficult to measure accurately [22–24], and moreso for diulte systems. Full scale deflection of the strain gauge mechanism on most commercial instruments is achieved at $\mathcal{O}(20N)$, which for a typical 50 mm cone corresponds to a stress of $\mathcal{O}(10^4)$ Pa whereas the stresses generated by these dilute dispersions are at least 2 orders of magnitude smaller than that. Further compounding the problem is the quadratically increasing inertial contribution to the normal force at high shear rates, $F_{inertial} = -3/20\rho(R\omega)^2$ where ρ is density, R is the radius of the tool and ω is the rotational velocity [25].

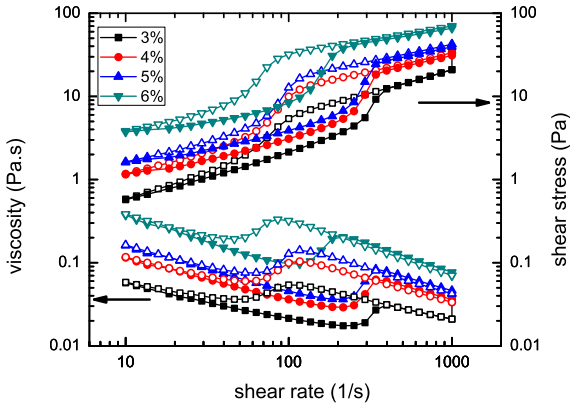

Fig. 2 Thixotropic loops for carbon black dispersion in a 1:1 tetradecane-mineral oil fluid. Filled symbols are for ascending sweeps, open symbols for descending runs.

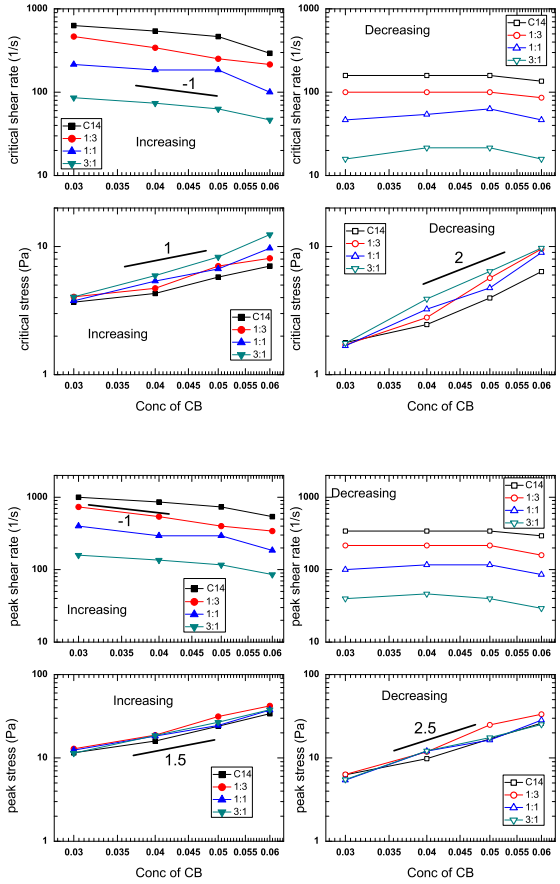

Fig. 3 Composition dependence of critical stress and shear rate at the ascending and descending shear thickening transitions (top) and peaks (bottom). The lines in the graphs serve as guides, with slopes as indicated by the value of the exponents in the text.

Nonetheless, by making careful corrections to the normal stress signal measured using the ARES LS-1 instrument and averaging over several runs, we were able to accurately and reproducibly resolve the first normal stress difference (N_1) behavior in the shear thickening regime of tetradecane dispersions of carbon black, Figure 5. We find that N_1 shows a marked upturn at the shear thickening transition followed by a peak and eventual downturn. The marked upturn, however, was only visible for more concentrated samples, $\varphi > 4$ wt.%. This behavior is in contrast to the negative first normal stress differences that develop on hydrocluster driven thickening in concentrated hard sphere systems [26,24]. The downturn in the normal stresses at high shear rates does not appear to be related to any improper inertial correction of the data. It appears to be coincident with the peak of the shear thickening response in the more concentrated samples, but its origin is currently unexplained.

In order to understand the origins of the observed rheology, we imaged the microstructures that were present at different points of the steady flow curve for a dilute alumina dispersion, which permitted reasonably good optical contrast, as shown in Figure 6. At low shear rates, in the shear thinning regime, the system consists of large "chunks" of the broken gel. In the structuring regime, we observe the appearance of vorticity aligned flocs which adopt a log-rolling motion. These flocs gradually break down in the shear thinning regime that follows the structuring regime, eventually forming a collection of densified clusters. Finally, in the shear thickening regime, these dense clusters are broken up and the system consists of small, finely dispersed aggregates that dramatically increase the optical density of the sample. Shear thickening in the dispersion materials is caused by the increase in the effective fraction of the particles when large clusters are broken up and dispersed. These results are in excellent agreement with the observed structures in carbon black systems, published previously [18] and are analogous to a "cluster dilation" model advanced to explain a negative thixotropy in concentrated ferric oxide suspensions [27]. This mechanism is markedly different than the hydrocluster formation which drives thickening in non-flocculating suspensions. It is expressly dictated by the fractal nature of the particles which allows them to form compact aggregates due to interpenetration as it were, of the highly structured particle surfaces and should be a general mechanism across many types of fumed particles.

While flow curves measured at higher shear rates, $\dot{\gamma} > 10^0$ s^{-1}, are smooth and of excellent reproducibility, data collected at lower shear rates were less con-

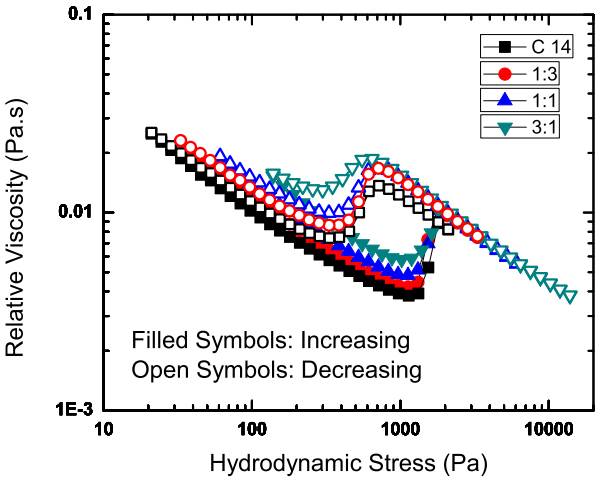

Fig. 4 Ascending and descending sweep flow curves for 4 wt.% carbon black in oil-tetradecane (C14) mixtures of 0:4, 1:3, 1:1 and 3:1 compositions. The shear rate is reduced to the hydrodynamic stress by multiplying by the viscosity of the solvent, producing superposition of the relative-viscosities, indicating that shear thickening is controlled by a critical stress.

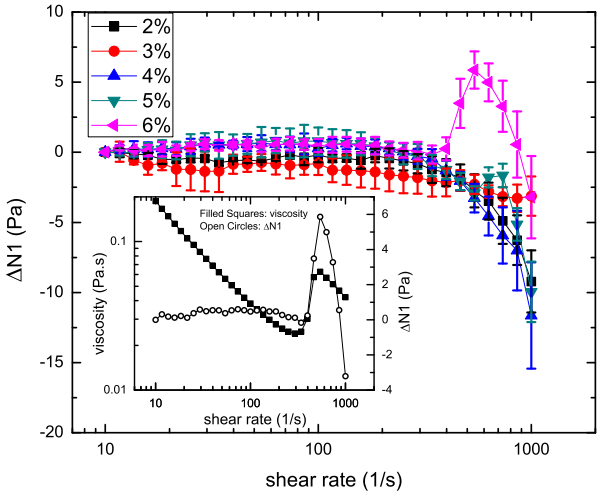

Fig. 5 Normal stress data on ascending rate sweeps of carbon black dispersions in Tetradecane, taken as the difference with respect to the value at the lowest shear rate, $\Delta N_1(\dot{\gamma}) = N_1(\dot{\gamma}) - N_1(\dot{\gamma} = 10)$. Data are averaged over 4 separate runs, and the error bar represents the standard deviation in the normal stress at each data point. Inset shows the viscosity and normal stress behavior the 6 wt.% sample where the co-location of the shear thickening transition and the sharp upturn in N_1 is clearly visible.

sistent from run to run, and rather noisy [28]. In some cases for instance, the viscosity was observed to decrease monotonically with decreasing shear rate. One possibility is that wall slip occurs at shear rates far below 10^0 s^{-1}, as it is well known to occur in the yielding of sticky colloidal systems such as these [29]. Transient stress measurements on step-wise reduction of shear rates at different gaps in the parallel-plate geometry

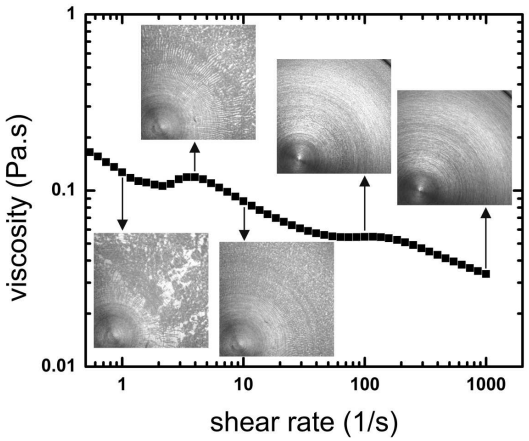

Fig. 6 Microstructure at different shear rates for a 2 wt.% Alumina dispersion in 3:1 oil:tetradecane fluid using a 1° 50 mm cone. Field of view is 1 cm x 1 cm

however, suggest that wall slip is not a large factor [30,31] and that homogeneous flow is achieved at the shear rates considered, Figure 7. Further, the use of tools covered by roughened surfaces was found to preserve features of the flow curve, and did not eliminate the unusually low and decreasing viscosities sometimes observed on decreasing shear rates in the low shear rate regime.

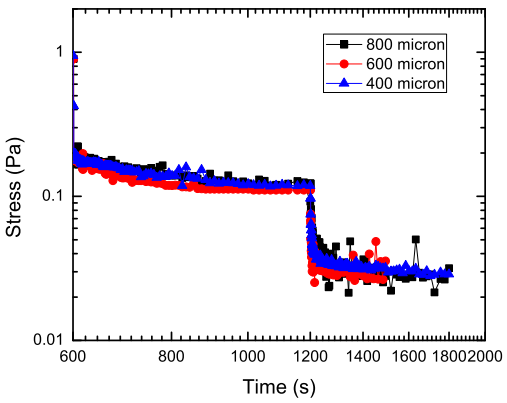

Fig. 7 Transient stress measurements on 4 wt.% carbon black in tetradecane. Data are for step-wise reductions in shear rate from 100 to 2.5 and 0.5 s−1 gaps of 400, 600 and 800 μm in the parallel plate geometry.

It appears instead that sedimentation of the particles at low shear rates is responsible for the lack of consistency of the data. The use of sequential ascending and descending runs with long equilibration delays allows substantial time for sedimentation to occur, and is exacerbated at low shear rates where shear-

induced re-suspension cannot occur. Indeed, consistent smooth flow curve data were only obtained when the Couette geometry was used, as shown in Figure 8. In this geometry, the effects of sedimentation are mitigated by the large height (34 mm) of the tool. We observe good agreement between ascending and descending flow curves in the low shear rate limit, all the way down to 10^{-3} s^{-1} and the small increases in viscosity in the structuring regime are consistently present. This is in contrast to data measured in the cone-plate geometry where the effects of sedimentation are disproportionately amplified. It should be stressed that these data in the Couette were measured on the ARES-LS1 instrument using 2 directions per data point, with equilibration and torque-averaging times of 60 and 10 seconds per direction, resulting in a high degree of confidence that these are equilibrium flow curves.

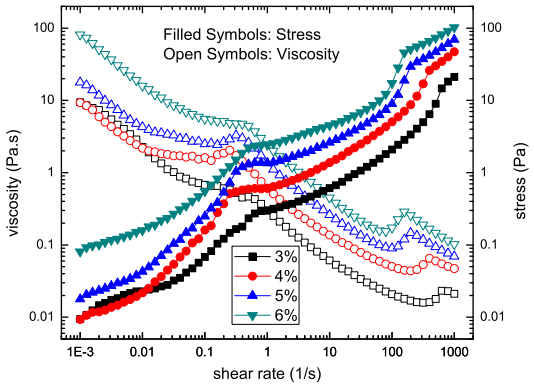

Fig. 8 Ascending rate flow curves for carbon black dispersions in 3:1 oil:tetradecane fluid measured in the Couette geometry on ARES-LS1 instrument.

3.2 Vorticity Aligned Structure Formation

Vorticity alignment of structures in complex fluids appears to be a quite general phenomenon, having been observed in several associating systems under flow such as thixotropic clay gels [32], nanotube suspensions [33] and attractive emulsion droplets [34]. Their appearance is usually associated with a negative first normal stress difference. The observation of these structures in steady-state flow in carbon black and alumina dispersions is thus not surprising, although we did not observe consistently measurable negative normal stress differences in the structuring regime of our system. However the rheology associated with their formation here appears to be unique as their appearance is concurrent with a slight increase in the apparent viscosity of the system though Pasquali et al. have observed a small Newtonian plateau coincident with the formation of vorticity aligned emulsion droplet aggregates. While the exact mechanism of the viscosity effect remains unknown, it may stem from the significant occlusion of the tool cross-section by the cylindrical flocs. Our measurements show that the floc width is approximately equal to the gap of the tool which, assuming a circular cross section, implies that the flocs span the tool gap. This would give rise to lubrication stresses in the flow of fluid in the small spaces between the tool and floc surfaces and may be at the origin of the observed viscosity behavior.

The stability of the vorticity aligned structures is strongly dependent on gap size. As seen in the data of Figure 6, the structures are not present beyond a certain radial distance from the center of the cone. While they are present as steady state structures, they also form strikingly and then gradually breakup as a transient response in the deformation of shear thickened suspensions of at a fixed shear rate or on quenches from high shear rate thickening flow into the shear thinning regime of the flow curve [28]. This is shown in Figure 9 for a 2% alumina suspension. Here, as also reported for a flocculated nanotube system [33], the structure formation is strongly parameterized by the gap size. In the current system, their formation may be governed by the rapid aggregation of the small finely dispersed clusters produced in the shear thickening flow. Given the R^3 dependence of torque on radial distance in the cone-plate geometry, [35], the contribution from the log-like flocs to the apparent viscosity is small as the structures are destabilized at larger radial distances from the cone center. The use of the parallel plate geometry suffers from the radial dependence of the shear rate and so the rheology of these systems would best be studied as a function of gap size in the Couette geometry.

3.3 Gel Elasticity

Given the differences observed in suspension microstructure between regimes delineated by $\dot{\gamma}_c$, the critical shear thickening transition, it can be expected that the mechanical properties of the gels formed after cessation of pre-shear should differ as well. Dynamic measurements were carried out in the cone-plate geometry on the MCR instrument on carbon black suspensions in 3:1 blends of mineral oil with tetradecane. The samples were found to exhibit either a very small or immeasurable frequency dependence of the elastic modulus, Figure 10. The strain dependence of the moduli

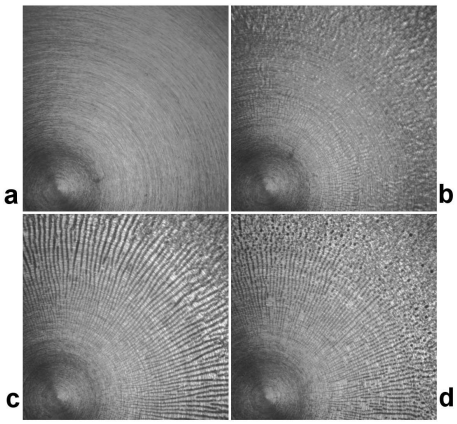

Fig. 9 Vorticity aligned flocs in rolling flow in 2% alumina in 50 mm, 1° cone-plate. Sample was quenched from from $\dot{\gamma} = 1000\text{s}^{-1}$ to 10 s^{-1}. Images are taken from (a) through (d) at 0, 4, 18 and 78 seconds after the rate quench. Field of view is 1 cm x 1 cm.

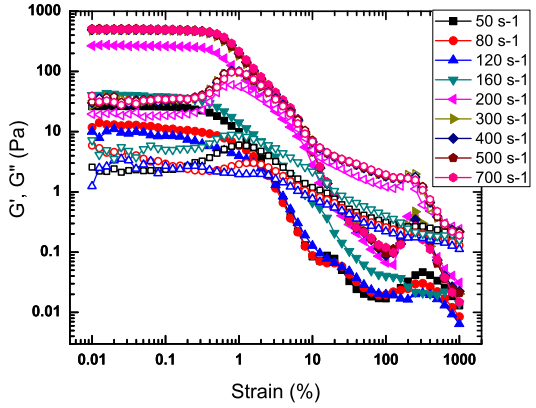

Fig. 11 Strain sweeps on samples subjected to different pre-shear flows. 5% carbon black in 3:1 oil:tetradecane fluid.

is characteristic of soft glassy materials, with a pronounced upturn in the loss modulus, G'', on yielding of the network, Figure 11. The yield strains appear to increase for samples produced at higher shear rates, but the uncertainty in accurately extracting a yield strain makes it difficult to asses this quantitatively. At very large strains, $\gamma \sim$ 100-1000%, there are small increases in the two moduli. This corresponds with the structuring regime observed in steady flow experiments and the dynamic shear rate, $\gamma\omega$, is similar to the steady flow rate in the steady measurements for these samples. Aging was not observed in these samples and the modulus remained steady over $\approx$ the period of observation (1 hour), including a 15 minute sweep performed to check the time evolution of the modulus, Figure 12.

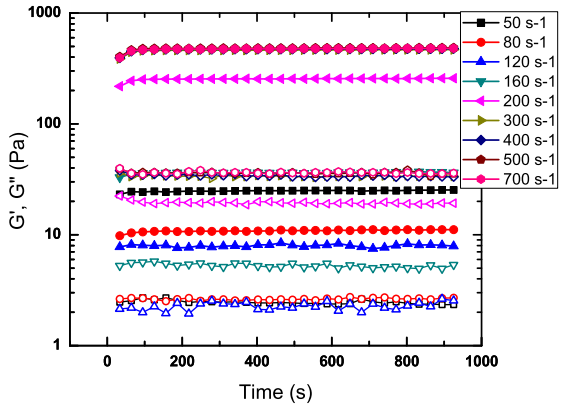

Fig. 12 Storage and loss moduli of gels remain constant during measurement after 30 minute quiescent gelation. 5% carbon black in 3:1 oil:tetradecane fluid.

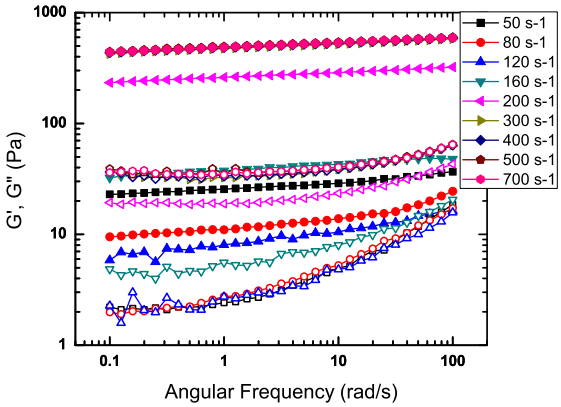

Fig. 10 Frequency sweeps on samples subjected to different pre-shear flows. 5% carbon black in 3:1 oil:tetradecane fluid.

When considered as a function of the pre-shear stress, the elastic moduli display a marked power-law dependence for samples sheared above the shear thickening transition, scaling roughly as $G' \sim \sigma^2$, Figure 13. The strong dependence of the modulus on the pre-stress can be understood in terms of the gel structure that results upon cessation of shear. Gelation in these fluids is very rapid and the system presents an elastic modulus at the shortest measurable times after cessation of shear, t $\leq$ 5s. The gel modulus can then be viewed as simply a cohesive energy density [36] that results from the contact between clusters, the dimensions of which are set by the magnitude of the pre-shear stress.

The shear force on a cluster of radius R_c is distributed over N_s particles in the plane of shear of the cluster. The cluster, a fractal object, has $N_s \sim R_c^{d_f - 1}$ where d_f is the fractal dimension of the cluster. The at-

tractive interaction, U, between particles of dimension a balances this force such that the dependence of the cluster size on the shear stress is as given in Equation 2.

$$R_c^{d_f-3} \sim \frac{4\pi\sigma a}{U} \tag{2}$$

The elastic modulus is then given as $G' \sim \nu U$ where ν is the number density of clusters, $\nu \sim \varphi/R_c^{d_f}$. Thus,

$$G' \sim \phi\sigma^{\frac{d_f}{3-d_f}} \tag{3}$$

Assuming a value of 2 for the fractal dimension, this suggests that $G' \sim \sigma^2\phi$. Replotting the data in these reduced terms produces a good agreement between our simple scaling model and the data, Figure 13. The data is in rough agreement with experimental data on that demonstrates that the number of particles in a floc scales roughly as $N_c \sim \sigma^{-1}$ [37]. The choice of fractal dimension for the gel is reasonable, though somewhat arbitrary. Previous data on carbon black gels in 100% tetradecane fluid were better fit assuming a fractal dimension of 1.8. Curiously, the maximum elastic moduli of those gels were a factor of $\approx$ 3X higher than that achieved in the more viscous 3:1 oil:tetradecane fluid.

The results reported here shed some light on the work of Raghavan et al. in which the structural recovery of flocculated silica gels was studied as a function of time after large-amplitude oscillatory shear at different strains. They observed that the recovered modulus was strongly dependent on the strain applied, and that higher moduli were obtained if the samples were subjected to larger strains. They hypothesize that the difference is due to changes in the network structure, with smaller strains leading to rearrangement of the network into larger flocs, leading to a reduction in the number of "crosslinks" in the systems. This reasoning is in line with our findings. Our experiments have provided direct imaging that supports these assertions, and our scaling model accounts well for the data. The strong dependence of the modulus on the pre-shear stress calls into question the utility of the composition scaling of the modulus, $G' \sim \varphi^\alpha$ as a metric for the interaction strength in fumed colloidal systems. The standard procedure in experimental investigations is to apply a high rate pre-shear to 'initialize' the system, and then to measure the modulus but our data suggest that a more accurate approach would involve applying a composition scaled stress as the pre-shear.

The gelation that occurs on cessation of shear flow can be thought of as a "mechanical quench" of the

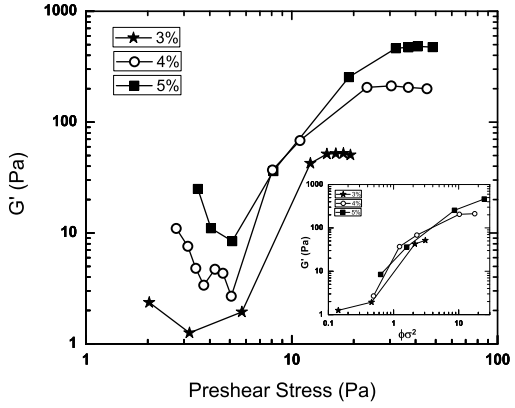

Fig. 13 Elastic modulus of gels as function of pre-shear stress. Inset: data re-scaled according to Equation 3

dispersion from a freely flowing gel state into an arrested gel. In the alumina and carbon black materials studied here, for the volume fractions considered, gelation was very rapid, and samples display a finite modulus at the earliest measurable times ($\sim$ 5 s) after cessation of shear. Such near-immediate establishment of a percolated network after stopping flow has also been observed in silica gels [19] as well as suspensions of ferric-oxide [38]. This sol-gel transition can be expected to involve the display of residual or internal stresses as the gel network is deformed with respect to an equilibrium relaxed configuration. Such a stress, σ_i, should be proportional to the modulus of the system, through the amount of the out-of-equilibrium strain, γ_d, and should relax gradually in time [39]. The concept of such a "trapped stress" has been invoked to account for the strange dynamics observed in the aging of some glassy systems [40,41]. Measurement of stress decays after stress-jumps enable a decoupling of the viscous and elastic stress components and have been made on a variety of systems in the short time limit ($\leq 10^0$ s) [31, 42]. Using the fast-feedback control loop of our MCR instrument, we successfully measured these stresses after a fast quench (0.1 s duration) to the stationary state out to 10^3 s after cessation of shear, Figure 14. Measurements are conducted on carbon black dispersions in 3:1 oil:tetradecane fluids that have been subjected to different pre-shears. We find a weak power law decay, with $\sigma_i \sim t^{-0.1}$ across all shear rates, with the initial value of the shear stress, $\sigma_i(t = 0.1)$ on the order of 1-10% of the pre-shear stress. Reversing the direction of the pre-shear correspondingly switches the sign of the residual stress. The data are in excellent agreement with the time-dependence observed for suspensions of carbon black in tetradecane measured on an

AR-G2 instrument [18], suggesting that this approach can be satisfactorily used if very short time data is not required. The direct proportionality expected between the residual stress and the modulus is confirmed by these measurements, Figure 15.

A standard stress relaxation measurement in the linear regime of course yields such a direct correspondence between σ and G' as well, but in the current experiment, the stresses that are relaxing are not measured in response to a step-strain on an equilibrium structure, but arise solely on the rapid rate quench of the system. These stresses are of non-trivial magnitude. For example, for gels prepared at 700 s^{-1}, the residual stress just after cessation of shear is about 3 Pa, Figure 14 whereas the yield stress measured in the strain sweep, Figure 11 is only about 2.5 Pa. The presence of residual stresses in these systems should be taken into account in designing stress relaxation experiments as the stress resulting from the applied step-strain in the experiment is superposed on the existing residual stress. This can lead to artifacts such as negative stresses on strain-controlled instruments such as the ARES which automatically offset the transducer at the start of the step-strain. At present we are unable to reconcile the presence of internal stresses that are significant in comparison to measured yield stresses in these materials. More detailed studies are required. Here, the MCR instrument is particularly well suited to these studies as it permits specification of the braking time over which the sample is quenched from the flowing to the stationary state.

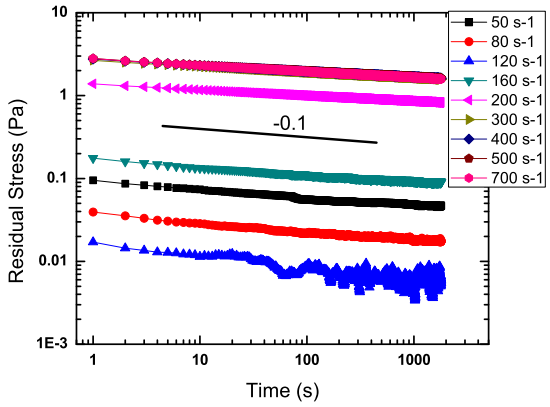

Fig. 14 Residual stresses measured on cessation of shear from different shear rates.

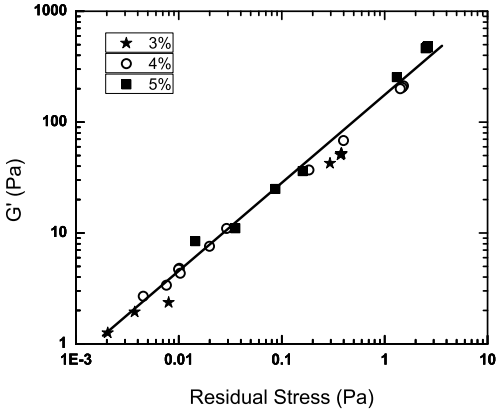

Fig. 15 Modulus of gels as a function of the magnitude of the residual stress, measured just after cessation of shear.

4 Conclusion

The observation of shear thickening in flocculating systems is a rather surprising result. It is a modest effect relative to the shear thickening and jamming that occur in dense hard sphere systems. The data are highly reproducible and indicate that the transition is controlled by a critical stress and is concurrent with an upturn in the first normal stress difference. Shear thickening here can be well understood in terms of the breakdown of clusters and the resultant increase in the effective volume fraction of particles in the fluid. This effect is exactly as a result of the unique fractal morphology of the colloidal particle concerned and so the mechanism is not relevant for Euclidean solid particles. The strong dependence of the gel modulus on the pre-shear stress is properly rationalized in terms of the cluster number density that results from the pre-shear flow. This has important implications in applications where fumed colloidal particles are used as fillers in fluids, including polymers, as the elasticity of the fluid can be strongly influenced by the mixing conditions. Surfactants can be used to sterically modulate the attractive interaction between particles, and this would be expected to alter the shear thickening behavior. In preliminary experiments, we have observed that the critical shear thickening transition shifts to lower stresses, as would be expected for decreased floc strength due to the presence of the surfactant. Finally, the dynamics of the rolling motion of the log-like flocs is of interest. A careful analysis may yield insight into rheology observed in the structuring regime.

Acknowledgements The authors would like to acknowledge Dr. Chanjoong Kim and Prof. David Weitz of Harvard Univer-

sity for fruitful discussions, and funding from the National Science Foundation under grant number CBET-0828905.

References

1. H. Barnes, Journal of Rheology **33**, 329 (1989)
2. L. Bergstrom, Colloids and Surfaces a-Physicochemical and Engineering Aspects **133**(1-2), 151 (1998)
3. M.D. Chadwick, J.W. Goodwin, B. Vincent, E.J. Lawson, P.D.A. Mills, Colloids and Surfaces a-Physicochemical and Engineering Aspects **196**(2-3), 235 (2002)
4. M.K. Chow, C.F. Zukoski, Journal of Rheology **39**(1), 15 (1995)
5. J. Bender, N.J. Wagner, Journal of Rheology **40**(5), 899 (1996)
6. B.J. Maranzano, N.J. Wagner, Journal of Rheology **45**(5), 1205 (2001)
7. J.F. Brady, G. Bossis, Journal of Fluid Mechanics **155**(JUN), 105 (1985)
8. J.R. Melrose, Faraday Discussions **123**, 355 (2003)
9. J.R. Melrose, J.H. vanVliet, R.C. Ball, Physical Review Letters **77**(22), 4660 (1996)
10. V. Gopalakrishnan, C.F. Zukoski, Journal of Rheology **48**(6), 1321 (2004)
11. S.R. Raghavan, S.A. Khan, Journal of Colloid and Interface Science **185**(1), 57 (1997)
12. P. Coussot, Soft Matter **3**(5), 528 (2007)
13. W. Smith, C. Zukoski, Langmuir **20**(25), 11191 (2004)
14. J. Helsen, J. Teixeira, Colloid & Polymer Science **264**(7), 619 (1986)
15. S. Khan, N. Zoeller, Journal of Rheology **37**, 1225 (1993)
16. M.C. Grant, W.B. Russel, Phys. Rev. E **47**(4), 2606 (1993). DOI 10.1103/PhysRevE.47.2606
17. C. Fischer, C. Plummer, V. Michaud, P. Bourban, J. Månson, Rheologica Acta **46**(8), 1099 (2007)
18. C.O. Osuji, C. Kim, D.A. Weitz, Physical Review E **77**(6), 060402 (2008). DOI 10.1103/PhysRevE.77.060402
19. S. Raghavan, S. Khan, Journal of Rheology **39**(6), 1311 (1995)
20. M. Kawaguchi, M. Okuno, T. Kato, Langmuir **17**(20), 6041 (2001)
21. H. Barnes, Journal of Non-Newtonian Fluid Mechanics **70**(1-2), 1 (1997)
22. V.G. Kolli, E.J. Pollauf, F. Gadala-Maria, Journal of Rheology **46**(1), 321 (2002). DOI 10.1122/1.1428320
23. I.E. Zarraga, D.A. Hill, J. David T. Leighton, Journal of Rheology **44**(2), 185 (2000). DOI 10.1122/1.551083
24. A. Singh, P.R. Nott, Journal of Fluid Mechanics **490**, 293 (2003)
25. W. Kulicke, G. Kiss, R. Porter, Rheologica Acta **16**(5), 568 (1977)
26. A. Singh, P.R. Nott, Journal of Fluid Mechanics **412**, 279 (2000)
27. H. Kanai, T. Amari, Rheologica Acta **34**(3), 303 (1995)
28. C.O. Osuji, D.A. Weitz, Soft Matter **4**, 1388 (2008). DOI 10.1039/B716324J
29. H. Walls, S. Caines, A. Sanchez, S. Khan, Journal of Rheology **47**, 847 (2003)
30. A. Yoshimura, R.K. Prud'homme, Journal of Rheology **32**, 1 (1988)
31. K. Dullaert, J. Mewis, Journal of Colloid and Interface Science **287**(2), 542 (2005)
32. F. Pignon, A. Magnin, J.M. Piau, Physical Review Letters **79**, 4689 (1997)
33. S. Lin-Gibson, J.A. Pathak, E.A. Grulke, H. Wang, E.K. Hobbie, Physical Review Letters **92**, 048302 (2004)
34. A. Montesi, A.A. Pena, M. Pasquali, Physical Review Letters **92**, 058303 (2004)
35. C. Macosko, *Rheology: Principles, Measurements and Applications* (Wiley-VCH, 1994)
36. R.G. Larson, *The Structure and Rheology of Complex Fluids* (Oxford University Press, 1999)
37. R.C. Sonntag, W.B. Russel, Journal of Colloid and Interface Science **113**, 399 (1987)
38. H. Kanai, T. Amari, Rheologica Acta **32**(6), 539 (1993)
39. L. Ramos, L. Cipelletti, Physical Review Letters **94**(15), 158301 (2005)
40. R. Bandyopadhyay, D. Liang, H. Yardimci, D.A. Sessoms, M.A. Borthwick, S.G.J. Mochrie, J.L. Harden, R.L. Leheny, Physical Review Letters **93**, 228302 (2004)
41. M. Bellour, A. Knaebel, J.L. Harden, F. Lequeux, J.P. Munch, Physical Review E **67**, 031405 (2003)
42. B. Kaffashi, V.T. Obrien, M.E. Mackay, S.M. Underwood, Journal of Colloid and Interface Science **187**(1), 22 (1997)